


RESEARCH ARTICLE | APRIL 24 2023

On the elastodynamic properties of octet truss-based architected metamaterials

Mourad Oudich ; Edward Huang; Hyeonu Heo; ... et. al

 Check for updates

Appl. Phys. Lett. 122, 171701 (2023)

<https://doi.org/10.1063/5.0140673>


View
Online


Export
Citation

CrossMark

Articles You May Be Interested In

Ultra-stiff and ultra-light architected metamaterial for vibration mitigation

J Acoust Soc Am (October 2022)

The small-scale limits of electron beam melt additive manufactured Ti–6Al–4V octet-truss lattices

AIP Advances (September 2022)

Resonant ultrasound spectroscopy measurement and modeling of additively manufactured octet truss lattice cubes

J Acoust Soc Am (October 2022)

Downloaded from http://pubs.aip.org/apl/article-pdf/doi/10.1063/5.0140673/16967002/171701_1_5.0140673.pdf



Time to get excited.
Lock-in Amplifiers – from DC to 8.5 GHz

[Find out more](#)

 Zurich
Instruments

On the elastodynamic properties of octet truss-based architected metamaterials

Cite as: Appl. Phys. Lett. **122**, 171701 (2023); doi: [10.1063/5.0140673](https://doi.org/10.1063/5.0140673)

Submitted: 29 December 2022 · Accepted: 6 April 2023 ·

Published Online: 24 April 2023



View Online



Export Citation



CrossMark

Mourad Oudich,^{1,2,a)} Edward Huang,³ Hyeonu Heo,¹ Zhenpeng Xu,⁴ Huachen Cui,⁴ Nikhil JRK Gerard,¹ Xiaoyu (Rayne) Zheng,^{4,5,a)} and Yun Jing^{1,a)}

AFFILIATIONS

¹Graduate Program in Acoustics, The Pennsylvania State University, University Park, Pennsylvania 16802, USA

²Université de Lorraine, CNRS, Institut Jean Lamour, F-54000 Nancy, France

³William C. Enloe Magnet High School, Raleigh, North Carolina 27610, USA

⁴Department of Civil and Environmental Engineering, University of California, Los Angeles, California 90095, USA

⁵Department of Materials Science and Engineering, University of California, Berkeley, California 94720, USA

Note: This paper is part of the APL Special Collection on Fundamentals and Applications of Metamaterials: Breaking the Limits.

a) Authors to whom correspondence should be addressed: mourad.oudich@univ-lorraine.fr; rayne23@berkeley.edu; and yqj5201@psu.edu

ABSTRACT

Architected metamaterials have emerged as a central topic in materials science and mechanics, thanks to the rapid development of additive manufacturing techniques, which have enabled artificial materials with outstanding mechanical properties. This Letter seeks to investigate the elastodynamic behavior of octet truss lattices as an important type of architected metamaterials for high effective strength and vibration shielding. We design, fabricate, and experimentally characterize three types of octet truss structures, including two homogenous structures with either thin or thick struts and one hybrid structure with alternating strut thickness. High elastic wave transmission rate is observed for the lattice with thick struts, while strong vibration mitigation is captured from the homogenous octet truss structure with thin struts as well as the hybrid octet truss lattice, though the underlying mechanisms for attenuation are fundamentally different (viscoelasticity induced dampening vs bandgaps). Compressional tests are also conducted to evaluate the effective stiffness of the three lattices. This study could open an avenue toward multifunctional architected metamaterials for vibration shielding with high mechanical strength.

Published under an exclusive license by AIP Publishing. <https://doi.org/10.1063/5.0140673>

Architected metamaterials are engineered structures and/or material compositions that can provide unprecedented mechanical and dynamic properties—low density coupled with high strength and stiffness,^{1,2} negative Poisson's ratio,³ negative stiffness for energy absorption,^{4,5} negative thermal expansion coefficient,⁶ and vibration control.^{7–16} They are generally built with connected struts and masses in a sophisticated design configuration to achieve the above-mentioned behaviors and functionalities. In particular, octet truss-based architected metamaterial (OTAM)¹⁷ is a structure best known for its high strength-to-weight ratio due to its stretch-dominated architecture.¹⁸ The highly connected node networks in the OTAM structure provide outstanding stiffness with low density.¹ In addition, the deformation mechanism of OTAMs endows them with excellent energy absorption capability,^{19–21} therefore making them promising candidates for lightweight protection materials.²² While OTAMs have been primarily studied for their mechanical (quasi-static) properties, their

elastodynamic behaviors remain elusive in the context of stress wave propagation. Messener *et al.*²³ theoretically characterized the effective dynamic properties of a periodic octet truss structure by evaluating the elastic wave dispersion relation at the long-wavelength regime. Beyond this approximative dynamic description of the lattice based on homogenization theory, further investigation of the elastodynamic properties of OTAMs is important as they could be proven a useful multifunctional material for providing outstanding load resistance and vibration attenuation. This constitutes the motivation for this study.

Targeting multifunctional capability, several studies dealt with engineering lightweight architected metamaterials for sound and vibration control with high mechanical strength. These investigations included high stiffness panels for sound absorption^{24,25} and vibration attenuation with controllable Poisson's ratio²⁶ and mechanical strength.^{27,28} The present work focuses specifically on the octet truss lattice that presents outstanding mechanical strength but a limited

vibration attenuation ability. We seek to address this performance limitation of octet truss lattices for vibration mitigation by considering a hybrid design architecture.

There are two main mechanisms that could be at play for vibration attenuation: energy dissipation (e.g., due to the viscoelasticity of the intrinsic material) and reflection [due to the presence of bandgaps (BGs)]. In engineering applications, energy dissipation is the primary means for vibration attenuation (e.g., rubber vibration isolators). However, BG-based vibration reduction can potentially lead to a greater amount of transmission loss. Very recently, Aguzzi *et al.*^{29,30} investigated the wave dispersion for a plate made of octet truss lattice and showed BGs at low frequency. Although their plate-type octet truss structure shows promising performance for vibration mitigation, it was designed for controlling plate waves. In this present work, we consider the octet truss lattice as a truly 3D lattice (rather than a 2D plate structure) for bulk vibration mitigation, which is fundamentally different from that of Aguzzi *et al.*^{29,30} The bulk wave velocity is, in general, greater than that of plate waves when the plate thickness is comparable to wavelength. Consequently, the wave dispersion by a periodic lattice is produced at higher frequencies for bulk waves in comparison with the case of a plate structure. Our 3D OTAM lattices are designed for bulk wave dispersion and attenuation, where the challenge is to achieve these functionalities at low frequencies. Furthermore, we also consider hybrid OTAMs for the purpose of low frequency vibration shielding with BGs that, otherwise, would not exist at the specific period under study with the permissible strut size.

In this Letter, we study the OTAMs where particular attention is brought to the structural design and the lattice's elastodynamic properties to achieve vibration attenuation while maintaining its excellent mechanical property. Three designs of OTAM are considered: OTAM with thin struts, thick struts, and hybrid OTAM made by alternating octet truss units with thin and thick struts. For each OTAM design, the elastodynamic properties have been investigated using numerical analysis and experimental realization via a 3D printing technique followed by dynamic and static characterizations to evaluate its capability to attenuate vibration and its mechanical strength.

The three OTAMs are periodic lattices of octet truss units made of cylindrical struts (rods) having the same diameter [Fig. 1(a)]. The unit cell length (period) is $a = 1.5$ cm. Throughout this study, the material mechanical properties used in the numerical simulation are those of the polymeric material used in 3D printing, which are the density $\rho = 1175.5$ kg/m³, Young's modulus $E = 3$ GPa, and Poisson's ratio $\nu = 0.46$. To determine these properties, samples of the polymeric material were printed and tested on MTS Criterion—model 43 with 20 kN loadcell and video extensometer, MTS Systems. The specimen size follows the ASTM E8 standard tensile test method. At room temperature (22 °C), the tensile force on the specimen was measured with a load cell under 0.01 mm/s overhead displacement. Simultaneously, longitudinal and transverse strains were recorded by the video extensometer and used to determine Young's modulus and Poisson's ratio of the printed materials. Furthermore, as the used polymeric material is viscoelastic, we performed multifrequency dynamic tests to measure the dynamic modulus and the mechanical loss factor via Q800 dynamic mechanical analysis (DMA), TA Instruments. In a dynamic tension mode, an oscillating force was applied to the sample, and the sample's response to the force was analyzed via the time-temperature superposition analysis.³¹ Consequently, we considered

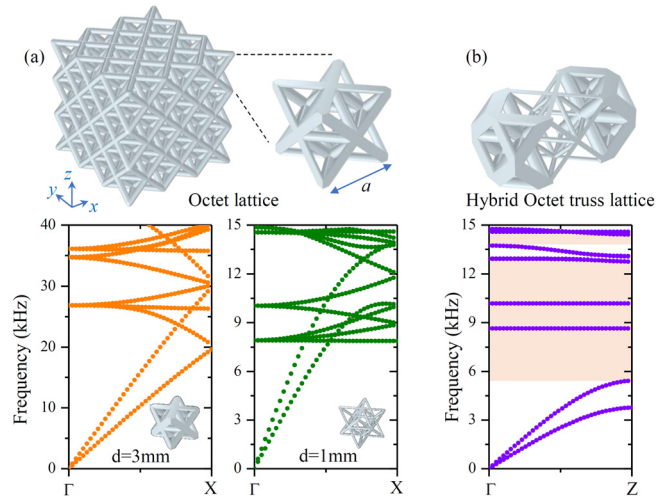


FIG. 1. (a) Octet truss lattice with unit cell (Upper panel). Band structures for the cases of struts diameter of 3 and 1 mm (bottom panel). (b) Hybrid octet truss lattice made of alternating octet truss unit cells with different struts diameters (1 and 3 mm). The band structure shows the appearance of BGs (bottom panel, shaded regions). Note the different frequency ranges in the band structures.

the approximate value of 0.12 for the loss factor in the numerical simulations for evaluating the wave transmission through the OTAMs and the hybrid OTAM.

We first calculated the dispersion curves for the three OTAM lattices by considering a unit cell (Fig. 1) using the eigenfrequency analysis in the commercial software COMSOL Multiphysics. The first OTAM was made of rods with a diameter of 3 mm [Fig. 1(a), bottom left panel], the second one was with 1 mm diameter [Fig. 1(a), bottom right panel], and the third OTAM was made by alternating octet truss units with rod diameters 1 and 3 mm [Fig. 1(b)]. We refer to this third lattice as the hybrid OTAM (HOTAM). The two OTAMs are periodic in all three directions in space, so an octet truss unit cell was considered with periodic boundary conditions in all three directions for the band structure calculation. For the HOTAM, since the periodic alternation of the octet truss units with different diameters is along the x direction in space [Fig. 1(b)], the periodicity is 3 cm along this direction, while it is 1.5 cm along y and z directions. We limit our dispersion calculation to the Γ - Z direction in the irreducible Brillouin zone, which corresponds to the propagation direction along the octet truss units' alternation in the HOTAM, because the wave transmission will be studied only in this same direction later in the study. We note that this direction is consistent with the loading direction of octet truss lattices. The full band structure of the HOTAM lattice is presented in the [supplementary material](#).

In the case of thick rods OTAM (3 mm diameter), the band structure shows no dispersion up to 20 kHz, while for frequencies higher than 20 kHz, the lattice displays strong band dispersion but with no BGs [Fig. 1(a), bottom left panel]. However, when considering the OTAM with thin rods (1 mm diameter), strong band dispersion is depicted starting from 7.87 kHz with no BG as well [Fig. 1(a), bottom right panel]. For the case of HOTAM, several BGs can be seen below 15 kHz with the lowest one extending from 5.4 to 8.6 kHz [Fig. 1(b)]. The alternation of the rods diameter from one octet truss unit to the

adjacent one induces a periodic change in the effective stiffness of the HOTAM as the octet truss units with thick rods display a higher effective stiffness than that of the units with thin rods. This makes the HOTAM a phononic crystal with BGs. These BGs are created by the mechanism of Bragg scattering caused by the periodicity of the lattice.³²

We then fabricated samples to study the dynamic and quasi-static behaviors of the three lattices. We chose to make samples of $5 \times 2 \times 2$ octet truss units [insets in Figs. 2(b)–2(d)]. The fabrication of the OTAM and HOTAM samples was made possible by stereolithography (SLA) using a Formlab Form 3 + 3D printer. All microstructures were fabricated with a specific orientation, approximately 30° tilted from the normal direction to the horizontal plane, to avoid internal support structures within the lattices from the 3D printing. The selected printing resolution had a layer thickness of $25 \mu\text{m}$. While the two OTAMs were made with struts of 1 and 3 mm diameters, the HOTAM was constructed by alternating rods diameter of the units starting with 3 mm at the base [see inset in Fig. 2(d)]. In addition to the lattice-based microstructure, the fabricated samples have plates with a thickness of 3 mm on both ends for the convenience of the experimental characterization. The samples were tested immediately after fabrication to preserve the initial constituent material stiffness as the material gets hardened over time, particularly when exposed to light. Three samples were fabricated for each design, which allowed us to evaluate the standard derivation of experimental results.

The elastic wave transmission measurements through the OTAM and HOTAM samples were carried out by connecting a K2004E01-SU

Mini Shaker into the plate on one end of the sample, and the shaker was connected to a function (signal) generator, PicoScope (series 5000), that facilitates the longitudinal wave excitations. The plate of the other end of the sample was connected to an accelerometer [PCB Piezotronics 352C67 (100 mV/g)] to measure the transmitted wave through the sample from one end to the other. The accelerometer was connected to a PCB Piezotronics ICP Sensor Signal Conditioner (482B11), which amplifies the acquired signal and transmits the data into a PicoScope (series 5000 oscilloscopes). The reference frequency of the PicoScope was programmed to drive the mechanical shaker to cycle from 2 to 15 kHz, at an amplitude of 60 mV, with an incrementation of 100 Hz every second [Fig. 2(a)].

The measured transmission curves for the OTAMs and HOTAM samples are presented in Figs. 2(b)–2(d), along with the numerically calculated transmission (via COMSOL) for the sake of comparison. In the case of OTAM with thick rods (3 mm diameter), relatively strong wave transmission is depicted in both measurement and simulation in the range of frequencies 2–15 kHz, except for the presence of a dip at 14.2 kHz, which is likely due to the anti-resonance of the plate in contact with the shaker [Fig. 2(b)]. This dip is also depicted but at a higher frequency (a little above 15 kHz) in the measurement. However, in the case of OTAM with thin rods (1 mm), the experimental and calculated transmissions show a significant drop from 6 kHz to higher frequencies [Fig. 2(c)], though the dispersion curve calculation does not show any presence of BGs [Fig. 1(a)]. This drop is caused by the viscoelastic loss of the used polymeric materials as thin rods support high order modes at this range of frequency that can be damped by the loss. Good agreement is found between simulation and measurement results. In the case of HOTAM, strong wave attenuation is observed between 6 and 12 kHz with relatively good agreement between the measured and calculated transmissions [Fig. 2(d)]. This wave attenuation is caused by the presence of the BG from the periodicity of the hybrid lattice. A discussion about the effect of viscoelasticity in HOTAM is presented in the [supplementary material](#). In summary, accessing wave attenuation with octet truss lattices below 15 kHz with the period of 1.5 cm can be achieved via the HOTAM using the BG or the OTAM with thin rods via viscoelasticity of the polymeric material. However, it is expected that the two samples would show different mechanical strengths.

In order to measure the effective mechanical properties of the three architected metamaterials, compressional tests were performed using QTest 100 (100 kN frame) with 10 kN loadcell, MTS Systems [Fig. 3(a)]. The experiment was conducted with 0.01 mm/s overhead displacement, while the reaction force was measured through the load cell at room temperature (22°C). Based on measured stress and strain, the effective stiffness and ultimate strength of each specimen were determined. Figures 3(b)–3(d) show the stress-strain curves for the OTAMs with rods thickness of 3 mm [Fig. 3(b)] and 1 mm [Fig. 3(c)] and for the HOTAM [Fig. 3(d)]. From these curves, we deduced the effective stiffness and the ultimate strength for the three structures, which are summarized in Table I. The 3D printed OTAM lattices were made of a strong polymer (Formlabs, clear resin). In the compression test, we observed that the stress of OTAM with thin rods reaches its peak value when the lattice reaches its elastic limit, after which stage the stress drops due to the buckling of the struts. For OTAM with thick rods, the lattice shows a typical ductile behavior, with fracture occurring at a high level of strain. No buckling was observed due to

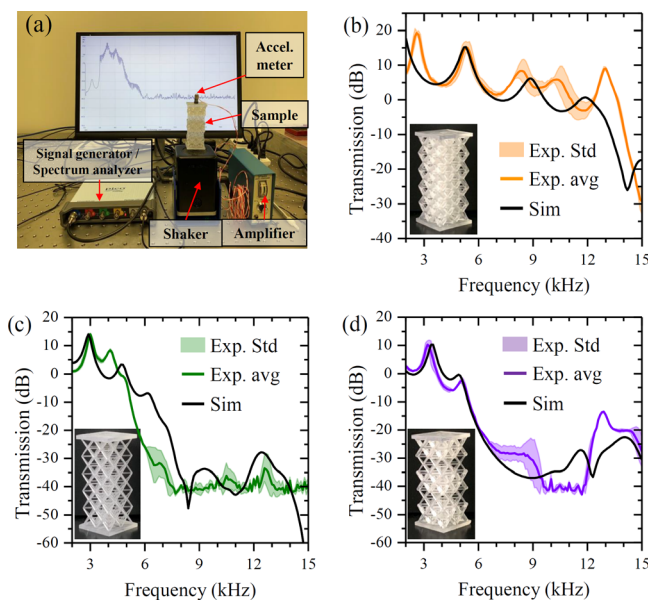


FIG. 2. (a) Experimental setup for measuring the elastic wave transmission through the OTAM and HOTAM samples. A shaker is used for wave excitation, and an accelerometer is used for measuring the transmitted wave. (b) and (c) Experimental measurements (colored solid lines) and numerical calculations (solid black lines) of the wave transmission as a function of the frequency for OTAMs with rods thicknesses 3 mm [orange line in (b)] and 1 mm [green line in (c)], and the HOTAM [purple line in (d)]. The shaded region on the colored curves marks the shaded error bar deduced from standard deviation of the repeated measurements.

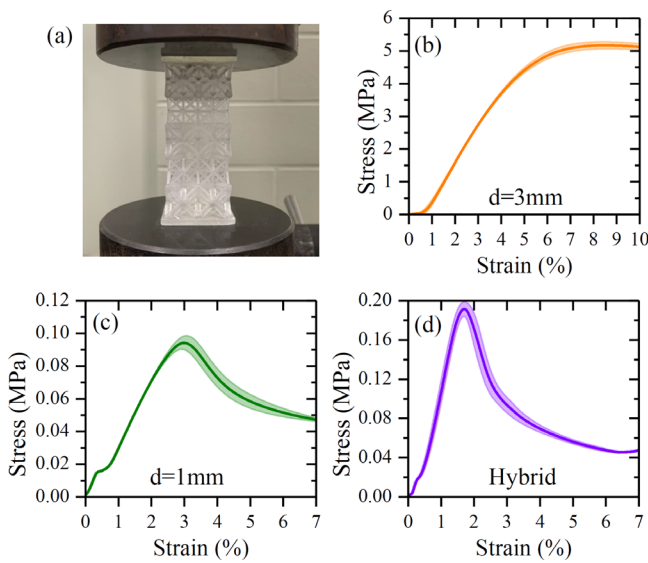


FIG. 3. (a) Compressional test on the OTAM and HOTAM. (b)–(d) Compression test results as the measured stress–strain curve for the OTAMs with rods diameter 3 (b) and 1 mm (c) as well as for the HOTAM (d).

the low aspect ratio of the struts. For the HOTAM, we observed local buckling at the layer with thinner rods after the linear region. With further increase in strain, local fractures were observed at the junction of thin and thick rods (see videos of the tests in the [supplementary material](#)). Furthermore, the more brittle response of HOTAM compared with OTAM with thick rods is mainly due to thin strut thickness and local rupture. For HOTAM, the buckling stress of the lattice depends on the thin struts rather than the thick struts if considering a compression direction of (1,0,0), as presented in this work. Therefore, the HOTAM shows lower stiffness than the OTAM with thick rods. We observed some local fractures during the compression test of HOTAM, which can be attributed to stress concentrations at the junction of thin and thick rods.

From [Table I](#), it is clear that the effective stiffness and strength of the OTAM with thick rods (3 mm diameter) are one order of magnitude higher than those of the OTAM with thin rods (1 mm) and the HOTAM. Nevertheless, although the stiffness of the HOTAM is 4 times higher than that of the OTAM with 1 mm rod diameter, the density of the HOTAM is 4.6 times larger, which leads to a slightly

TABLE I. Effective mechanical properties of the OTAMs and HOTAM samples.

	OTAM with 3 mm	OTAM with 1 mm	HOTAM
Effective density ρ_{eff} (kg/m ³)	444.67	62.82	291.51
Relative density ($\bar{\rho} = \rho_{\text{eff}}/\rho_0$)	37.83%	5.34%	24.80%
Effective stiffness E_{eff} (MPa)	121.98	4.20	16.71
Normalized stiffness $E_{\text{eff}}/\bar{\rho}$ (MPa)	322.46	78.60	67.38
Ultimate strength (MPa)	5.33	0.11	0.20

lower normalized stiffness of the HOTAM in comparison to the OTAM. In addition, the ultimate strength of HOTAM remains higher than that of the OTAM. In short, though the OTAM with thick rods displays the highest mechanical strength, its ability to shield elastic waves is limited in comparison to the OTAM with thin rods, which has the drawback of having a relatively poor mechanical strength. A combination between the two OTAMs, which gives the HOTAM, increases the ultimate strength while providing the ability to shield vibration based on the mechanism of BG.

In conclusion, we have investigated the mechanical strength and elastodynamic properties of three types of octet truss lattices: two OTAMs with homogenous struts diameters and a hybrid OTAM with alternating octet truss units with different rod diameters. The OTAM with thick rods (3 mm) displays high effective stiffness and ultimate strength but has a low capability for attenuating vibration at low frequencies (below 13 kHz). However, although the rod's diameter can be lowered to enable the OTAM capability for elastic wave shielding via the viscoelastic effect, its stiffness and strength are lowered by almost two orders of magnitude, which may hinder its usability. Combining the two OTAM designs by alternating the octet truss units with different rod diameters, on the other hand, increases the effective stiffness of the lattice while endowing the structure with the ability of elastic wave mitigation through the mechanism of BG. The present study could open routes toward heterogeneous design of 3D architected lattices with increased mechanical strength while providing opportunities for vibration control.

See the [supplementary material](#) for the study on the effect of viscoelasticity, the characterization of the loss factor of the polymeric material, the full band structure of the HOTAM, and the multimedia views of the compression tests.

We would like to thank Garrett Corso at the Materials Research Institute, Penn State University, for performing the material's tensile tests and DMA. We also thank Dr. Henrietta Tsosie at the Department of Engineering Science and Mechanics, Penn State University, for assisting with the compression test. Y.J. thanks the NSF DMREF for the support through CMMI 2119545. X.Z. thanks the NSF DMREF for the support through CMMI 2119643 and AFOSR (No. FA9550-18-1-0299).

AUTHOR DECLARATIONS

Conflict of Interest

The authors have no conflicts to disclose.

Author Contributions

Mourad Oudich: Conceptualization (equal); Investigation (equal); Methodology (equal); Writing – original draft (equal); Writing – review & editing (equal). **Edward Huang:** Investigation (equal). **Hyeonu Heo:** Investigation (equal); Methodology (equal); Writing – original draft (equal); Writing – review & editing (equal). **Zhenpeng Xu:** Investigation (equal); Methodology (equal); Resources (equal); Writing – review & editing (equal). **Huachen Cui:** Investigation (equal); Writing – review & editing (equal). **Nikhil JRK Gerard:** Investigation (equal); Methodology (equal); Writing – review & editing (equal). **Xiaoyu (Rayne) Zheng:** Funding acquisition (equal);

Resources (equal); Supervision (equal); Writing – review & editing (equal). **Yun Jing:** Conceptualization (equal); Funding acquisition (equal); Methodology (equal); Resources (equal); Supervision (equal); Writing – review & editing (equal).

DATA AVAILABILITY

The data that support the findings of this study are available from the corresponding author upon reasonable request.

REFERENCES

- ¹X. Zheng, H. Lee, T. H. Weisgraber, M. Shusteff, J. DeOtte, E. B. Duoss, J. D. Kuntz, M. M. Biener, Q. Ge, J. A. Jackson, S. O. Kucheyev, N. X. Fang, and C. M. Spadaccini, *Science* **344**, 1373 (2014).
- ²X. Zheng, W. Smith, J. Jackson, B. Moran, H. Cui, D. Chen, J. Ye, N. Fang, N. Rodriguez, T. Weisgraber, and C. M. Spadaccini, *Nat. Mater.* **15**, 1100 (2016).
- ³D. Chen and X. Zheng, *Sci. Rep.* **8**, 9139 (2018).
- ⁴C. S. Ha, R. S. Lakes, and M. E. Plesha, *Int. J. Solids Struct.* **178–179**, 127 (2019).
- ⁵C. S. Ha, R. S. Lakes, and M. E. Plesha, *Mater. Des.* **141**, 426 (2018).
- ⁶H. Heo, S. Li, H. Bao, and J. Ju, *Adv. Eng. Mater.* **21**, 1900225 (2019).
- ⁷S. Taniker and C. Yilmaz, *Int. J. Solids Struct.* **72**, 88 (2015).
- ⁸K. H. Matlack, A. Bauhofer, S. Krödel, A. Palermo, and C. Daraio, *Proc. Natl. Acad. Sci. U. S. A.* **113**, 8386 (2016).
- ⁹L. D'Alessandro, E. Belloni, R. Ardito, F. Braghin, and A. Corigliano, *Appl. Phys. Lett.* **111**, 231902 (2017).
- ¹⁰F. Warmuth, M. Wormser, and C. Körner, *Sci. Rep.* **7**, 3843 (2017).
- ¹¹L. D'Alessandro, V. Zega, R. Ardito, and A. Corigliano, *Sci. Rep.* **8**, 2262 (2018).
- ¹²W. Elmadih, D. Chronopoulos, W. P. Syam, I. Maskery, H. Meng, and R. K. Leach, *Sci. Rep.* **9**, 11503 (2019).
- ¹³X. Fei, L. Jin, X. Zhang, X. Li, and M. Lu, *Appl. Phys. Lett.* **116**, 021902 (2020).
- ¹⁴N. J. Gerard, M. Oudich, Z. Xu, D. Yao, H. Cui, C. J. Naify, A. Ikei, C. A. Rohde, X. (Rayne) Zheng, and Y. Jing, *Phys. Rev. Appl.* **16**, 024015 (2021).
- ¹⁵Muhammad and C. W. Lim, *Sci. Rep.* **11**, 7137 (2021).
- ¹⁶Z. Xu, R. Hensleigh, N. J. Gerard, H. Cui, M. Oudich, W. Chen, Y. Jing, and X. (Rayne) Zheng, *Addit. Manuf.* **47**, 102321 (2021).
- ¹⁷V. S. Deshpande, N. A. Fleck, and M. F. Ashby, *J. Mech. Phys. Solids* **49**, 1747–1769 (2001).
- ¹⁸L. Dong, V. Deshpande, and H. Wadley, *Int. J. Solids Struct.* **60–61**, 107 (2015).
- ¹⁹T. Tancogne-Dejean, A. B. Spierings, and D. Mohr, *Acta Mater.* **116**, 14 (2016).
- ²⁰M. Mieszala, M. Hasegawa, G. Guillonneau, J. Bauer, R. Raghavan, C. Frantz, O. Kraft, S. Mischler, J. Michler, and L. Philippe, *Small* **13**, 1602514 (2017).
- ²¹Z. Xu, C. S. Ha, R. Kadam, J. Lindahl, S. Kim, H. F. Wu, V. Kunc, and X. Zheng, *Addit. Manuf.* **32**, 101106 (2020).
- ²²S. Mora, N. M. Pugno, and D. Misseroni, *Mater. Today* **59**, 107 (2022).
- ²³M. C. Messner, M. I. Barham, M. Kumar, and N. R. Barton, *Int. J. Solids Struct.* **73–74**, 55 (2015).
- ²⁴B. Han, Z.-J. Zhang, Q.-C. Zhang, Q. Zhang, T. J. Lu, and B.-H. Lu, *Extreme Mech. Lett.* **10**, 58 (2017).
- ²⁵Y. Tang, S. Ren, H. Meng, F. Xin, L. Huang, T. Chen, C. Zhang, and T. J. Lu, *Sci. Rep.* **7**, 43340 (2017).
- ²⁶Y. Chen, T. Li, F. Scarpa, and L. Wang, *Phys. Rev. Appl.* **7**, 024012 (2017).
- ²⁷A. S. Phani, J. Woodhouse, and N. A. Fleck, *J. Acoust. Soc. Am.* **119**, 1995 (2006).
- ²⁸I. Arretche and K. H. Matlack, *Front. Mater.* **5**, 68 (2018).
- ²⁹G. Aguzzi, C. Kanellopoulos, R. Wiltshaw, R. V. Craster, E. N. Chatzi, and A. Colombi, *Sci. Rep.* **12**, 1088 (2022).
- ³⁰G. Aguzzi, H. R. Thomsen, A. Hejazi Nooghabi, R. Wiltshaw, R. V. Craster, E. N. Chatzi, and A. Colombi, *Appl. Phys. Lett.* **121**, 201702 (2022).
- ³¹C. Pasini, N. Inverardi, D. Battini, G. Scalet, S. Marconi, F. Auricchio, and S. Pandini, *Smart Mater. Struct.* **31**, 095021 (2022).
- ³²M. Oudich, N. J. Gerard, Y. Deng, and Y. Jing, *Adv. Funct. Mater.* **33**, 2206309 (2023).